Precise 6D RTK Positioning System for UAV-based Near-Field Antenna Measurements

Patrick Henkel*, Andreas Sperl*, Ulrich Mittmann*, Torsten Fritzel§, Rüdiger Strauss§, Hans Steiner §
*ANavS GmbH: Munich, Germany, {patrick.henkel, andreas.sperl, ulrich.mittmann}@anavs.de
§AeroXess UG: Munich, Germany, {torsten.fritzel, ruediger.strauss}@aeroxess.com

***Abstract*—Near-field antenna measurements with an Unmanned Aerial Vehicle (UAV) require an accurate 3D position and 3D attitude information. In this paper, we estimate the position and velocity of the UAV, the quaternion that describes its attitude, the carrier phase integer ambiguities related to both the attitude and position, and the accelerometer bias with a Kalman filter. The raw measurements were obtained from the ANavS Multi-Sensor RTK module with its 3 Multi-frequency, Multi-GNSS receivers and a MEMS-based Inertial Measurement Unit (IMU). We used the UAV of AeroXess to validate our method and achieved a centimeter-level positioning accuracy in both static and kinematic conditions.**

***Index Terms*—UAV, UAS, localization, GNSS, GPS, Galileo, RTK, attitude determination, pose estimation, sensor fusion.**

I. Introduction

Unmanned Aerial Vehicles (UAV) have a broad range of applications: The professional UAV market targets aerial surveying and mapping, aerial surveillance and security, aerial inspection of infrastructure, and aerial delivery of goods. The accurate knowledge of the pose (position and attitude) of the UAV is essential for most of these applications. Global Navigation Satellite Systems (GNSS) such as GPS, Galileo, GLONASS and Beidou provide pseudorange, carrier phase and Doppler measurements at the receiver for positioning. The carrier phase can be tracked with a noise level of few millimeters to centimeters. However, the carrier phase is periodic with a wavelength of only 19 cm and, therefore requires an ambiguity resolution. The fixing of the carrier phase ambiguities from float to integer numbers has been a large research topic for more than 2 decades. The popular LAMBDA method of Teunissen [1] is the standard method for ambiguity fixing today.

The accuracy and convergence time of the position solution can be substantially improved by using measurements or corrections from a GNSS reference station. The corrections of a network of GNSS reference stations can also be extrapolated to the location of the UAV. This smart concept of virtual reference stations is presented by Landau et al. in [2]. Real-Time Kinematic (RTK) positioning refers to differential carrier phase based positioning with integer ambiguity resolution. The first low-cost RTK positioning for UAVs was presented by Stempfhuber and Buchholz in [3].

The performance of the RTK positioning can be enhanced by the integration of additional sensors. The Multi-Sensor RTK (MS-RTK) module of ANavS includes 3 Multi-frequency, Multi-GNSS receivers, a 3D accelerometer, a 3D gyroscope and a barometer. It performs the synchronization of all raw data as well as the RTK positioning and sensor fusion, and is described by Heinrich et al. in [4]. Krause et al. additionally integrated barometric height information into the RTK positioning for fast ambiguity refixing in [5]. Henkel et al. further used visual localization an a given map within the RTK positioning in [6].

II. Measurement Models

In this section, we briefly introduce the models for the differential carrier phase and pseudorange measurements of two GNSS receivers. A GNSS receiver includes a Delay Locked Loop (DLL) and a Phase Locked Loop (PLL) that provide the pseudorange measurements $\rho^k_{u,m}$ and carrier phase measurements $\lambda_m\varphi^k_{u,m}$ of user u on frequency $m \in \{1,\ldots,M\}$ of satellite $k \in \{1,\ldots,K\}$. The observations depend on the satellite positions and clock offsets. The satellites provide estimates of their position $\hat{\vec{x}}^{\,k}_u$ and clock offset $\delta\hat{\tau}^k$, that are used to correct the measurements [7]:

$$\begin{aligned}\lambda_m\tilde{\varphi}^k_{u,m} &:= \lambda_m\varphi^k_{u,m} + \vec{e}^{\,k}_u\hat{\vec{x}}^{\,k}_u + c\delta\hat{\tau}^k \quad \forall\, k,m \\ \tilde{\rho}^k_{u,m} &:= \rho^k_{u,m} + \vec{e}^{\,k}_u\hat{\vec{x}}^{\,k}_u + c\delta\hat{\tau}^k \quad \forall\, k,m \end{aligned} \tag{1}$$

where $\vec{e}^{\,k}_u$ is the normalized direction vector pointing from satellite k to receiver u and c denotes the speed of light. Moreover, the coordinates of the reference station are known. Thus, the measurements of the reference station are corrected:

$$\begin{aligned}\lambda_m\tilde{\varphi}^k_{r,m} &:= \lambda_m\varphi^k_{r,m} - \|\hat{\vec{x}}_r - \hat{\vec{x}}^{\,k}\| + c\delta\hat{\tau}^k \quad \forall\, k,m \\ \tilde{\rho}^k_{r,m} &:= \rho^k_{r,m} - \|\hat{\vec{x}}_r - \hat{\vec{x}}^{\,k}\| + c\delta\hat{\tau}^k \quad \forall\, k,m. \end{aligned} \tag{2}$$

In the next step, double differences (DD) of these corrected measurements are formed to eliminate atmospheric errors and satellite position and clock errors and biases:

$$\begin{aligned}\lambda_m\tilde{\varphi}^{kl}_{ur,m} &:= \lambda_m\left((\tilde{\varphi}^k_{u,m} - \tilde{\varphi}^l_{u,m}) - (\tilde{\varphi}^k_{r,m} - \tilde{\varphi}^l_{r,m})\right) \\ &= \vec{e}^{\,kl}_u\vec{b}_{ur} + \lambda_m N^{kl}_{ur,m} + \lambda_m\Delta\varphi^{kl}_{\mathrm{MP}_{ur,m}} + \varepsilon^{kl}_{ur,m},\end{aligned} \tag{3}$$

which depends on the relative position $\vec{b}_{ur}$ (also called baseline) between the receivers u and r, the carrier wavelength λ_m, the DD integer ambiguities $N^{kl}_{ur,m}$, the DD carrier phase multipath $\Delta\varphi^{kl}_{\mathrm{MP}_{ur,m}}$ and the DD phase noise $\varepsilon^{kl}_{ur,m}$.

Similarly, DD pseudoranges are formed as:

$$\begin{aligned}\tilde{\rho}^{kl}_{ur,m} &:= \left((\tilde{\rho}^{k}_{u,m} - \tilde{\rho}^{l}_{u,m}) - (\tilde{\rho}^{k}_{r,m} - \tilde{\rho}^{l}_{r,m})\right) \\ &= \vec{e}^{\,kl}_{u}\vec{b}_{ur} + \Delta\rho^{kl}_{\mathrm{MP}_{ur,m}} + \eta^{kl}_{ur,m}, \end{aligned} \quad (4)$$

with the DD pseudorange multipath $\Delta\rho^{kl}_{\mathrm{MP}_{ur,m}}$ and the DD pseudorange noise $\eta^{kl}_{ur,m}$.

III. Joint RTK and attitude determination with GNSS/ INS tight coupling

We use 3 GNSS receivers on the UAV for attitude determination and one additional reference station on the ground for RTK positioning. The 3 GNSS receivers on the UAV span two attitude baselines that are indexed by 1 and 2. The carrier phase and pseudorange measurements from the RTK baseline and both attitude baselines are stacked at epoch n in a single measurement vector as:

$$\begin{aligned} z_n^{\mathrm{GNSS}} &= \big((\lambda_1\tilde{\varphi}_{\mathrm{RTK},1})^{\mathrm{T}} \dots (\lambda_M\tilde{\varphi}_{\mathrm{RTK},M})^{\mathrm{T}}, \\ &\quad (\tilde{\rho}_{\mathrm{RTK},1})^{\mathrm{T}} \dots (\tilde{\rho}_{\mathrm{RTK},M})^{\mathrm{T}}, \\ &\quad (\lambda_1\tilde{\varphi}_{\mathrm{ATT}_1,1})^{\mathrm{T}}, (\lambda_1\tilde{\varphi}_{\mathrm{ATT}_2,1})^{\mathrm{T}}, \dots \\ &\quad (\lambda_M\tilde{\varphi}_{\mathrm{ATT}_1,M})^{\mathrm{T}}, (\lambda_M\tilde{\varphi}_{\mathrm{ATT}_2,M})^{\mathrm{T}}, \\ &\quad (\tilde{\rho}_{\mathrm{ATT}_1,1})^{\mathrm{T}}, (\tilde{\rho}_{\mathrm{ATT}_2,1})^{\mathrm{T}}, \dots \\ &\quad (\tilde{\rho}_{\mathrm{ATT}_1,M})^{\mathrm{T}}, (\tilde{\rho}_{\mathrm{ATT}_2,M})^{\mathrm{T}}\big)^{\mathrm{T}}, \end{aligned} \quad (5)$$

where the component vectors (e.g. $\lambda_1\tilde{\varphi}_{\mathrm{RTK},1}$) include the DD measurements from all used satellites of a certain baseline and frequency.

Similarly, the IMU measurements of the acceleration $\vec{a}^{\,\mathrm{b}}$ in the body-frame and of the angular rates $\vec{\omega}^{\mathrm{b}}_{\mathrm{ib}}$ of the body-frame w.r.t. the inertial-frame are stacked in a single IMU measurement vector as:

$$z_n^{\mathrm{IMU}} = \left((\vec{a}^{\,\mathrm{b}}(t_n))^{\mathrm{T}}, (\vec{\omega}^{\mathrm{b}}_{\mathrm{ib}}(t_n))^{\mathrm{T}}\right)^{\mathrm{T}}. \quad (6)$$

The state vector includes all unknown parameters of both the RTK and attitude baselines at time t_n, i.e.

$$x_n = \left((\vec{b}^{\,\mathrm{n}}_{\mathrm{RTK}})^{\mathrm{T}}, (\vec{v}^{\,\mathrm{n}})^{\mathrm{T}}, N^{\mathrm{T}}_{\mathrm{RTK}}, N^{\mathrm{T}}_{\mathrm{ATT}}, q^{\mathrm{n}}_{\mathrm{b}}, (b_{a^{\mathrm{b}}})^{\mathrm{T}}\right)^{\mathrm{T}}, \quad (7)$$

with the following notations:

$\vec{b}_{\mathrm{RTK}}$	3D baseline vector between UAV and reference station in local (North-East-Down, NED) navigation-frame
$\vec{v}^{\,\mathrm{n}}$	3D velocity vector of UAV
N_{RTK}	DD integer ambiguities from RTK baseline of all used satellites and frequencies
N_{ATT}	DD integer ambiguities from attitude baseline of all used satellites and frequencies
$q^{\mathrm{n}}_{\mathrm{b}}$	quaternion for rotation from body-frame to navigation-frame
$b_{a^{\mathrm{b}}}$	bias of accelerometer measurement

The state vector is predicted from its previous estimate with the help of the IMU measurements, and given by:

$$\hat{x}^{-}_n = f\left(\hat{x}^{+}_{n-1}, z^{\mathrm{IMU}}_n, z^{\mathrm{IMU}}_{n-1}\right), \quad (8)$$

with the non-linear prediction function $f(\cdot)$ being introduced for each state parameter in the following lines. The RTK baseline at epoch n is linear predicted using the velocity information:

$$\vec{b}^{\,\mathrm{n}}_{\mathrm{RTK},n} = \vec{b}^{\,\mathrm{n}}_{\mathrm{RTK},n-1} + \frac{1}{2}\left(\vec{v}^{\,\mathrm{n}}_{n} + \vec{v}^{\,\mathrm{n}}_{n-1}\right)\Delta t, \quad (9)$$

where Δt is the time between two subsequent state predictions with IMU measurements. The velocity is integrated with the acceleration $\vec{a}^{\,\mathrm{n}}_n$ (being obtained from the accelerometer and pre-corrected for gravity and biases), i.e.

$$\begin{aligned}\vec{v}^{\,\mathrm{n}}_{n} &= \vec{v}^{\,\mathrm{n}}_{n-1} + \frac{1}{2}\left(\vec{a}^{\,\mathrm{n}}_{n} + \vec{a}^{\,\mathrm{n}}_{n-1}\right)\Delta t \\ &= \vec{v}^{\,\mathrm{n}}_{n-1} + \frac{1}{2}\left(R^{\mathrm{n}}_{\mathrm{b},n}\vec{a}^{\,\mathrm{b}}_{n} + R^{\mathrm{n}}_{\mathrm{b},n-1}\vec{a}^{\,\mathrm{b}}_{n-1}\right)\Delta t. \end{aligned} \quad (10)$$

Plugging Eq. (10) into (9) yields

$$\begin{aligned}\vec{b}^{\,\mathrm{n}}_{\mathrm{RTK},n} &= \vec{b}^{\,\mathrm{n}}_{\mathrm{RTK},n-1} + \vec{v}^{\,\mathrm{n}}_{n-1}\Delta t \\ &\quad + \frac{1}{2}\left(R^{\mathrm{n}}_{\mathrm{b},n}\vec{a}^{\,\mathrm{b}}_{n} + R^{\mathrm{n}}_{\mathrm{b},n-1}\vec{a}^{\,\mathrm{b}}_{n-1}\right)\frac{\Delta t^2}{2}, \end{aligned} \quad (11)$$

with the rotation matrix $R^{\mathrm{n}}_{\mathrm{b},n}$ from the body-frame to the navigation-frame. The rotation can also be expressed in terms of the quaternion $q^{\mathrm{n}}_{\mathrm{b},n}$ as derived by Solà in [8]:

$$\vec{a}^{\,\mathrm{n}}_{n} = R^{\mathrm{n}}_{\mathrm{b},n}\vec{a}^{\,\mathrm{b}}_{n} = q^{\mathrm{n}}_{\mathrm{b},n} \otimes \vec{a}^{\,\mathrm{b}}_{n} \otimes \left(q^{\mathrm{n}}_{\mathrm{b},n}\right)^{*}, \quad (12)$$

where $*$ denotes the conjugate of the quaternion.

The quaternion at epoch n is obtained from the quaternion of the previous epoch with the help of the angular rate measurements $\vec{\omega}^{\mathrm{b}}_{\mathrm{ib},n}$ of the body-frame. The prediction of the quaternion is derived by Solà in [8] and given by:

$$q^{\mathrm{n}}_{\mathrm{b},n} = q^{\mathrm{n}}_{\mathrm{b},n-1} \otimes \left(q\left(\bar{\vec{\omega}}^{\mathrm{b}}_{\mathrm{ib}}\Delta t\right) + \frac{\Delta t^2}{24}\begin{pmatrix} 0 \\ \vec{\omega}^{\mathrm{b}}_{\mathrm{ib},n-1} \times \vec{\omega}^{\mathrm{b}}_{\mathrm{ib},n} \end{pmatrix}\right), \quad (13)$$

with the mean angular rate

$$\bar{\vec{\omega}}^{\mathrm{b}}_{\mathrm{ib}} = \frac{\vec{\omega}^{\mathrm{b}}_{\mathrm{ib},n-1} + \vec{\omega}^{\mathrm{b}}_{\mathrm{ib,n}}}{2} \quad (14)$$

and the quaternion

$$q\left(\bar{\vec{\omega}}^{\mathrm{b}}_{\mathrm{ib}}\Delta t\right) = \begin{pmatrix} \cos\left(\frac{1}{2}\|\bar{\vec{\omega}}^{\mathrm{b}}_{\mathrm{ib}}\|\Delta t\right) \\ \frac{\bar{\vec{\omega}}^{\mathrm{b}}_{\mathrm{ib}}}{\|\bar{\vec{\omega}}^{\mathrm{b}}_{\mathrm{ib}}\|}\sin\left(\frac{1}{2}\|\bar{\vec{\omega}}^{\mathrm{b}}_{\mathrm{ib}}\|\Delta t\right) \end{pmatrix} \quad (15)$$

that describes the rotation of the body-frame by $\bar{\vec{\omega}}^{\mathrm{b}}_{\mathrm{ib}}\Delta t$. The other state parameters (i.e. ambiguities of RTK and attitude baselines and accelerometer biases) are considered to be constant. The covariance matrix of all estimated states is propagated accordingly and given by:

$$\begin{aligned}\Sigma_{\hat{x}^{-}_n} &= \frac{\partial f(x_n)}{\partial x_n}\Sigma_{\hat{x}^{+}_{n-1}}\left(\frac{\partial f(x_n)}{\partial x_n}\right)^{\mathrm{T}} \\ &\quad + \frac{\partial f(x_n)}{z^{\mathrm{IMU}}_n}\Sigma_{z^{\mathrm{IMU}}_n}\left(\frac{\partial f(x_n)}{z^{\mathrm{IMU}}_n}\right)^{\mathrm{T}} \\ &\quad + \frac{\partial f(x_n)}{z^{\mathrm{IMU}}_{n-1}}\Sigma_{z^{\mathrm{IMU}}_{n-1}}\left(\frac{\partial f(x_n)}{z^{\mathrm{IMU}}_{n-1}}\right)^{\mathrm{T}} + \Sigma_{x_n} \end{aligned} \quad (16)$$

where $\frac{\partial f(x_n)}{\partial x_n}$ denotes the partial derivative of f with respect to x_n, $\Sigma_{\hat{x}^{+}_{n-1}}$ is the covariance matrix of the state update of the

previous epoch, $\Sigma_{z_n^{\mathrm{IMU}}}$ is the measurement noise covariance matrix of the current epoch, and Σ_{x_n} is the process noise covariance matrix.

The GNSS measurements of Eq. (5) are used to update the predicted states. The state update is obtained with a standard Kalman filter [9] and is given by

$$\hat{x}_n^+ = \hat{x}_n^- + K_n \left(z_n^{\mathrm{GNSS}} - H_n \hat{x}_n^- \right) \tag{17}$$

with the linearized mapping matrix $H_n = \frac{\partial z_n}{\partial x_n}$ and Kalman gain K_n. The covariance matrix of the updated state parameters is obtained by error propagation and given by

$$\begin{aligned} \Sigma_{\hat{x}_n^+} &= (1 - K_n H_n) \, \Sigma_{\hat{x}_n^-} \, (1 - K_n H_n)^{\mathrm{T}} \\ &\quad + K_n \Sigma_{z_n^{\mathrm{GNSS}}} (K_n)^{\mathrm{T}} = (1 - K_n H_n) \, \Sigma_{\hat{x}_n^-}, \end{aligned} \tag{18}$$

where the latter identity is obtained by plugging in the (optimized) Kalman gain that minimizes the variance of the updated state estimates.

The DD ambiguities of the RTK baseline are fixed with the famous LAMBDA method of Teunissen [1]. The attitude ambiguity fixing is significantly fastened by taking constraints on the baseline lengths [10] and relative orientation between the baselines [11]-[12] into account.

IV. Measurement Results

In this section, we describe our measurement set-up for 6D pose estimation with a UAV and the obtained measurement results.

A. Measurement set-up

The measurement set-up during the flight tests consisted of the following components:

- 1 UAV of AeroXess as shown in Fig. 1 and Fig. 2
- 3 High-Gain, Multipath-Suppression and Multi-frequency GNSS antennas of Tersus being mounted above the rotor blades of the UAV
- 1 Multi-Sensor RTK module of ANavS, see Fig. 3: The module was integrated into the UAV and includes:
  - 3 Multi-GNSS, Multi-frequency receivers
  - 1 industrial-grade MEMS IMU
  - 1 barometer
  - 1 GSM/ LTE module for receiving the RTK corrections from the reference station
  - 1 processor for running the RTK position and attitude determination with sensor fusion
- 1 RTCM reference station of ANavS, including:
  - 1 Multi-GNSS, Multi-frequency receiver
  - 1 GSM/ LTE module for transmitting the RTK corrections from the reference station to the Multi-Sensor RTK module
  - various interfaces (USB, Ethernet, CAN, WiFi) for outputting the position and attitude solution

The gyroscope bias was estimated during static initialization, and removed from the angular rate measurements.

Fig. 1. Photo of UAV of AeroXess on ground: 3 GNSS antennas are mounted above the rotor blades for an unobstructed reception of the GNSS signals.

Fig. 2. Photo of UAV of AeroXess in air during test flight at ANavS.

Fig. 3. Photo of Multi-Sensor Real-Time Kinematic (MS-RTK) positioning module of ANavS: The module includes 3 Multi-GNSS, Multi-frequency receivers for accurate position and attitude determination, an industrial-grade MEMS IMU, a barometer, a GSM/ LTE module for the reception of RTK corrections, a processor for running the RTK positioning with a tightly coupled sensor fusion and various other interfaces for additional sensors.

B. 6D Pose Solution

In this subsection, we show our 3D position and 3D attitude (roll, pitch and heading) solution. Fig. 4 shows the ANavS GUI

with the ground-track of the UAV in the right subfigure and the fixed phase residuals of all used GPS, Galileo, GLONASS and Beidou satellites in the left subfigure. The fixed phase residuals serve as accuracy information.

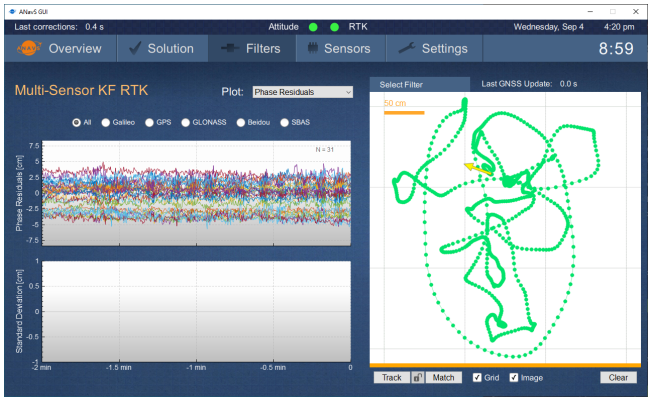

Fig. 4. Ground-track of UAV as shown on ANavS GUI. The left subfigure includes the fixed phase residuals; each line/ color refers to one satellite. The right subfigure shows the ground-track on a map. The noise levels of both the residuals and the position track are in the order of only 2 cm.

Fig. 5 shows the height of the UAV relative to the reference station, i.e. the UAV was at its static position almost 14 m below the reference station and during its flight up to 10 m above the ground. The similarity of the heights at the start and at the end is a good check for the overall consistency.

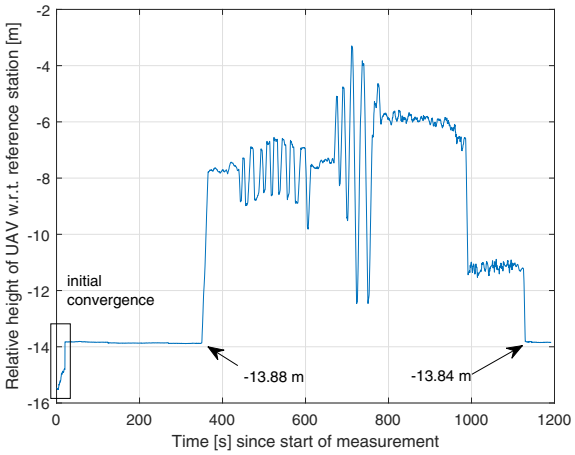

Fig. 5. Height of UAV relative to reference station.

Fig. 6 shows the estimated heading and Fig. 7 includes the estimated roll and pitch angles during the test flight. The noise level is in the order of only $0.1°$. The enlarged sections refer to periods of high dynamics with a rate of heading of up to $45°/s$ and pitch and roll angles of up to $\pm 20°$.

C. Accuracy Assessment

In this section, we describe the accuracy of the pose estimation of the UAV. The following two approaches were used to assess the accuracy without the need of a reference system:

- analysis of fixed carrier phase residuals
- re-fixing of ambiguities after landing of UAV and comparison of ambiguity-refixed solution with solution obtained directly after landing

The fixed phase residuals describe the consistency between the measured and calculated carrier phases for fixed ambiguities. As the number of phase measurements is especially for multiple GNSS constellations much larger than the number of unknown baseline coordinates, the fixed phase residuals are a quite good accuracy indicator. The second approach enables a detection of eventual errors (e.g. uncorrected cycle slips) that happened during the flight and remained in the solution.

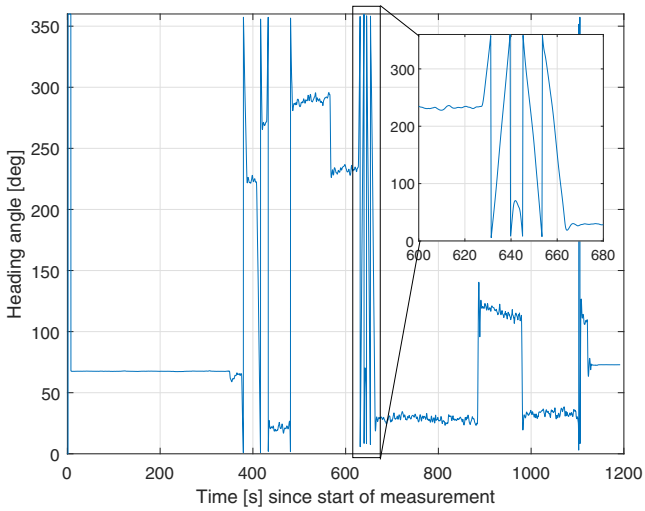

Fig. 6. Heading of UAV during test flight. The enlarged section in the upper right corner shows the heading during the turning of the UAV.

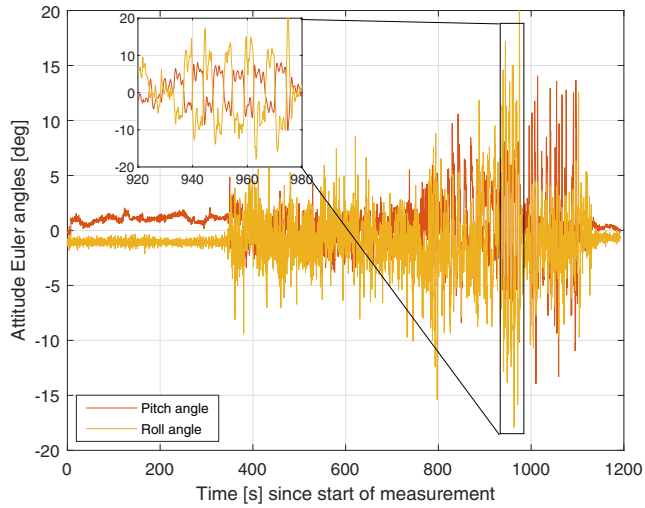

Fig. 7. Roll and pitch angle of UAV during test flight. The enlarged section refers to a period with higher pitch/ roll angle dynamics of up to $\pm 20°$.

We observed no jumps in the RTK and attitude solutions after ambiguity re-fixing, i.e. the attitude and RTK fixes were confirmed.

Fig. 8 shows the fixed phase residuals for the attitude baseline and Fig. 9 includes the fixed phase residuals for the RTK baseline. The residuals are typically in the order of a few centimeters, whereas the noise level is larger during the flight than during the static initialization. This can be explained by the adaption of the filter bandwidth within the GNSS receiver's tracking loop. The largest residual errors of the attitude solution occur during its highest dynamics in the pitch and roll angles. The inclined position of the UAV results in increased phase multipath and, thereby, increased phase residuals. Nevertheless, the Phase Locked Loops (PLLs) of most satellites preserved their phase lock, and both the attitude and RTK ambiguity fixes were kept throughout the flight.

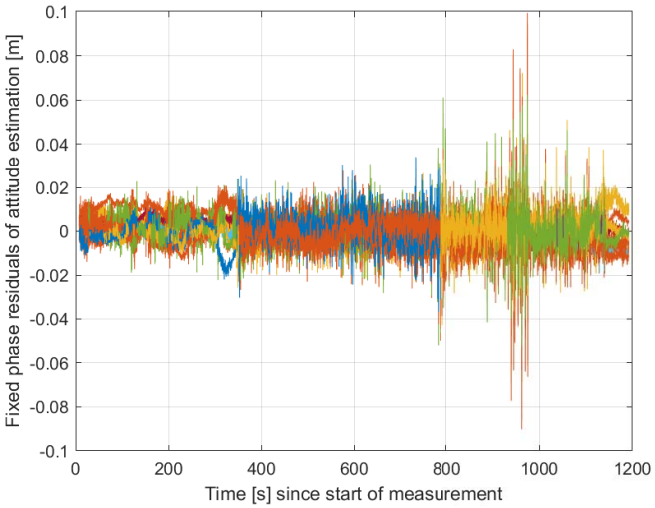

Fig. 8. Fixed phase residuals of attitude estimation for all used GPS, Galileo, GLONASS and Beidou satellites. The residuals are for all satellites for most of the time below 2 cm, which indicates a correct ambiguity fixing.

V. Conclusion

In this paper, we presented a joint RTK positioning and attitude determination with a tight coupling of GNSS and inertial measurements for UAVs. The position and velocity of the UAV, the quaternion describing its attitude, the carrier phase integer ambiguities related to both the attitude and position, and the accelerometer bias were estimated in a Kalman filter. We used the UAV of AeroXess to validate our method and achieved a centimeter-level positioning accuracy in both static and kinematic conditions.

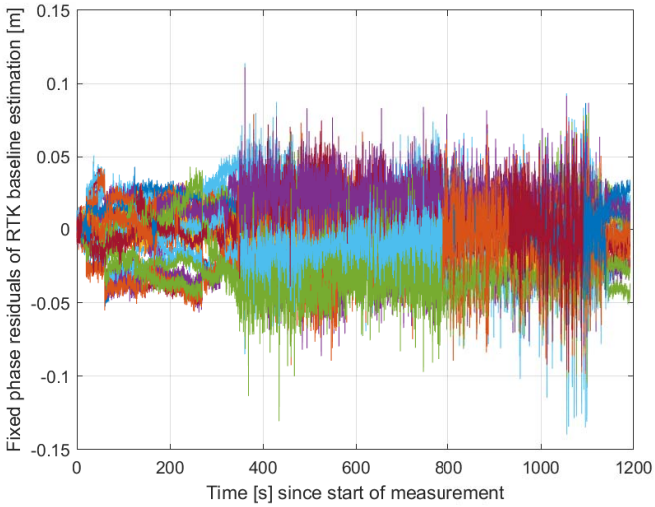

Fig. 9. Fixed phase residuals of RTK baseline estimation for all used GPS, Galileo, GLONASS and Beidou satellites. The residuals are for all satellites for most of the time below 5 cm, which indicates the accuracy of the position solution.

References

[1] P.J.G. Teunissen, "The Least-Squares Ambiguity Decorrelation Adjustment - A method for fast GPS ambiguity fixing", J. of Geodesy, vol. 70, pp. 65 – 82, 1995.

[2] H. Landau, U. Vollath and X. Chen, "Virtual Reference Station Systems", Journal of Global Positioning Systems, vol. 1, no. 2, pp. 137 – 143, 2002.

[3] W. Stempfhuber and M. Buchholz, "A Precise, Low-Cost RTK GNSS System for UAV Applications", Intern. Archives of the Photogrammetry, Remote Sensing and Spatial Information Sciences, Volume XXXVIII-1/C22, ISPRS Workshop, Zurich, Switzerland, Sep. 2011.

[4] M. Heinrich, A. Sperl, U. Mittmann and P. Henkel, "Reliable Multi-GNSS Real-Time Kinematic Positioning", IEEE Proc. of 60th Intern. Symp. ELMAR, Zadar, Croatia, pp. 103 – 108, Sep. 2018.

[5] J. Krause and P. Henkel, "Integration of barometric height into RTK Positioning for Fast Ambiguity Refixing", IEEE Proc. of 60th Intern. Symp. ELMAR, Zadar, Croatia, pp. 113 – 116, Sep. 2018.

[6] P. Henkel, A. Blum, C. Günther, "Precise RTK Positioning with GNSS, INS, Barometer and Vision", Proc. of 30th ION GNSS+, Portland, Oregon, USA, pp. 2290 – 2303, Sep. 2017.

[7] P. Misra and P. Enge, "Global Positioning System: Signals, Measurements, and Performance", Ganga-Jamuna Press, 2nd edition, 569 pp., 2011.

[8] J. Solà, "Quaternion kinematics for the error-state Kalman filter", Technical Report, Nr. IRI-TR-16-02, Universitat Politècnica de Catalunya (UPC), Barcelona, Spain, 70 pp., Sep. 2016.

[9] R.G. Brown and P.Y.C. Hwang, "Introduction to Random Signals and Applied Kalman Filtering with Matlab Exercises", Wiley, 4th edition, 400 pp., Feb. 2012.

[10] P.J.G. Teunissen, "Integer least-squares theory for the GNSS compass", J. of Geodesy, vol. 84, pp. 433 – 447, 2010.

[11] P. Henkel, P. Jurkowski and C. Günther, "Differential integer ambiguity resolution with Gaussian a priori knowledge and Kalman filtering", Proc. of 24th Int. Techn. Meeting of the ION, pp. 3881 – 3888, Sep. 2011.

[12] P. Henkel and C. Günther, "Reliable Integer Ambiguity Resolution: Multi-Frequency Code Carrier Linear Combinations and Statistical A Priori Knowledge of Attitude", Navigation, vol. 59, nr. 1, pp. 61 – 75, Mar. 2012.